XXIV Biennial Symposium on Measuring Techniques in Turbomachinery
Prague, Czech Republic, 29 - 31 August 2018
Paper No MTT2418B41

CTHWA DYNAMIC RESPONSE EFFECTS ON TURBULENCE MEASUREMENTS IN TURBOMACHINERY FLOWS

E. Boufidi, F. Fontaneto
"Jacques Chauvin" Laboratory
von Karman Institute for Fluid Dynamics
Rhode-St-Genèse, Belgium \
Université Catholique de Louvain,
Louvain-la-Neuve, Belgium

M. Cottes
Polytechnic department of engineering and architecture,
University of Udine, Italy

Keywords: turbulence, constant temperature hot-wire anemometry, dynamic response, turbomachinery

ABSTRACT

The effect of the dynamic response of CTHWAs on the measurement of turbulence is evaluated using a non-linear dynamic response model with synthetic turbulence signals as inputs. The errors in the measurement of the root mean square of the turbulence fluctuations, the integral length scale and the skewness are examined as a function of the input turbulence level and length scale and the anemometer's cut-off frequency. The first two errors mainly occur due to the limited bandwidth of the instrument and are a function of the ratio f_L/f_{cut}, where f_L is a characteristic frequency of the turbulence spectrum and f_{cut} the cut-off frequency of the anemometer. The last error is affected both by f_L/f_{cut} and the turbulence level and stems from the non-linearity of the system.

NOMENCLATURE

Symbols

a_w	temperature coefficient of resistance of wire material
c_w	heat capacity of wire material
d_w	wire diameter
E	CTHWA output voltage
E_b	offset voltage
E_{11}	1d turbulence energy spectrum
E_{33}	3d turbulence energy spectrum
f_{cut}	anemometer's cut-off frequency
G	amplifier gain
L	integral length scale
l_w	wire length
k	turbulent kinetic energy
k_a	thermal conductivity of air
M	wire time constant
M_b	bridge time constant
m_w	wire mass
M'	amplifier first order time constant
M''	amplifier second order time constant
Nu	Nusselt number
Pr	Prandtl number
Re	Reynolds number
R_{dec}	decade resistance
r_L	prongs, stem and cable resistance
R_{ref}	wire resistance at reference temperature
R_w	instantaneous wire resistance
R_0	wire resistance at flow temperature
R_1	bridge top left resistance
R_2	bridge top right resistance
R^*	wire resistance for a balanced bridge
$skew$	velocity signal skewness
T	integral time scale
Tu	turbulence intensity
$\overline{U}$	mean velocity
$\overline{u'}$	root mean square of velocity fluctuations

Greek letters

δ	voltage difference at bridge diagonal
ε	turbulent kinetic energy dissipation
η	kolmogorov length scale
κ	wavenumber
κ_1	wavenumber 1d
ρ	autocorrelation coefficient

Abbreviations

CTHWA	Constant temperature hot wire anemometry
FFT	Fast Fourier Transform
OHR	Overheat ratio

INTRODUCTION

A detailed characterization of turbulence in turbomachinery flows is essential to improve our understanding of the complex flow phenomena taking place, like heat transfer, mixing and loss generation. This characterization should extend beyond measuring just the intensity of the turbulent fluctuations, as the structure of the turbulent flowfield is known to have a significant effect [1]. Moreover, with the increasing use of high-fidelity CFD, like LES and DNS, the turbulent flowfield can be simulated, and therefore experimentally obtained higher-order turbulence statistics should be available for validation [2].

Constant Temperature Hot Wire Anemometry (CTHWA) is one of the most popular measurement tools for turbulence research thanks to its high

frequency response, high spatial resolution and good signal to noise ratio [3]. As every measurement technique, CTHWA is subject to different sources of errors including, but not limited to, calibration errors, errors due to mean fluid temperature variations and spatial resolution errors. The first two sources of errors have been extensively investigated. The filtering effect on the measured fluctuations due to the limited spatial resolution of the hot wire sensor has been extensively treated as well, and a review of different studies considering both isotropic and anisotropic turbulence can be found in [4].

Another source of errors is the dynamic response of CTHWAs. A CTHWA is composed of a hot wire probe and an electronic control unit, which consists of a Wheatstone bridge (the hot wire is part of the active leg of the bridge) and a feedback loop which adjusts the current to keep the temperature of the wire constant. The dynamic response of the system is, therefore, defined by the properties of the wire and the electronics. The common way to use CTHWA is to optimize the dynamic response for one operating point using the well-known square wave test and use static calibration laws to retrieve the instantaneous velocity, assuming a flat frequency response up to the cut-off frequency. This practice neglects the following sources of potential errors:

- The attenuation of fluctuations due to the heat conduction to the wire supports.
- The fact that the square wave test doesn't guarantee a flat frequency response up to the cut-off frequency and can result in amplification or damping of fluctuations.
- The non-linear nature of the governing equations.

The first point has been the subject of many investigations. As the conduction depends strongly on the wires' length to diameter ratio (lw/dw), different design criteria have been proposed for negligible attenuation. In their well-known study, Ligrani & Bradshaw [5] suggested that the length to diameter ratio should be higher than 200 for measurements in the viscous sublayer of a turbulent boundary layer, while, more recently, Hultmark et al. [6] proposed a new criterion that considers also the flow conditions and the wire material. Li [7], on the other hand, proposed a correction scheme using a digital filter to correct the effect of the attenuation a posteriori. The second point can be addressed by using a transfer function obtained by the square-wave test to correct the amplitude of the turbulence spectra, as suggested by Weiss et al. [8].

The third point is probably the most overlooked and it is the focus of the present investigation. Freymuth [9] developed the non-linear theory for CTHWA and demonstrated that for a well-tuned system and small fluctuations, their behavior can be sufficiently described by a third order linear equation. Thereafter, most investigations have focused on the linear theory and most experimental investigations neglect non-linear effects even for large fluctuations (see for example [10]). Freymuth [11] demonstrated that non-linear effects become important when the amplitude or the frequency of the fluctuations increase. Fluctuations as large as 50% of the mean velocity fall in the linear regime when their frequency is lower than 10% of the cut-off frequency of the anemometer. The non-linearity has a small effect on the intensity of the fluctuation but affects significantly odd moments like the skewness. Weiss et al. [12] verified Freymuth's [11] analytical results by solving numerically the system of non-linear equations and comparing with experimental results by electronic testing for three different anemometers. This non-linear behavior has been investigated for Constant Current Anemometry (CCA) by Comte-Bellot & Schon [13] and for Constant Voltage Anemometry (CVA) by Berson et al. [14]. Berson et al. [14] applied a post-processing algorithm to correct for nonlinearities by inversely solving the differential equations characterizing the CVA's response. No similar method is available for CCA or CTA in the author's knowledge.

In the present work, the non-linear model of Freymuth [9] and Weiss et al. [12] is employed to investigate the effects of the dynamic response on turbulence measurements, in flow conditions that are of interest for turbomachinery applications. Indeed, turbomachinery flows are characterized by large fluctuations and high turbulence levels. Even in laboratory testing with grid-generated turbulence, the trend is to increase the inlet turbulence intensity to more realistic levels, reaching values between 10% and 20%. Therefore, it is probable that the small-fluctuations assumption is not valid for many turbomachinery applications and that errors can occur to turbulence measurements due to the non-linearity of the CTHWA dynamic response. Unlike the previous works for CTA, where the effects of non-linearity were evaluated using sinusoidal fluctuations as input signal, synthetic turbulent flow fluctuations with varying levels of turbulence intensity and length scales are used in the present work.

CTHWA DYNAMIC RESPONSE MODEL

Governing equations

A CTHWA system is composed by a hot-wire probe and an electronic unit. A schematic of a simplified circuit is presented in Figure 1. The hot wire probe is connected at the bottom left leg of the Wheatstone bridge, with R_w the resistance of the wire and r_L the resistance of the prongs, stem and cable. The resistance R_{dec} is adjustable and it is used to set the desired overheat ratio. The resistance R_w is maintained constant by the

feedback amplifier, which adjusts the current to compensate for resistance fluctuations.

As mentioned before, the model of Freymuth [2] and Weiss et al. [8] is used to simulate the dynamic behavior of a CTHWA system. Three equations are needed: an equation for the Wheatstone bridge, one for the feedback amplifier and one for the wire.

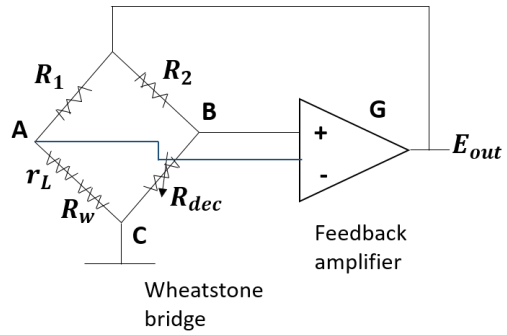

Figure 1: Simplified circuit of a CTHWA

The equation representing the behavior of the Wheatstone bridge is the following:

$$\delta = \frac{R_1(R^* - R_w)}{(R_1 + R^* + r_L)(R_1 + R_w + r_L)}E + M_B\frac{dE}{dt} \qquad (1)$$

where δ is the voltage difference at the bridge diagonal ($\delta = V_B - V_A$), see Figure (1)), R^* is the value of the operating wire resistance for a balanced bridge (the set value), E is the bridge output voltage and M_B a time constant used to take into account the high frequency effects due to reactive elements in the bridge.

The equation simulating the behavior of the amplifier is a second order linear equation:

$$M''\frac{d^2E}{dt^2} + M'\frac{dE}{dt} + E = G\delta + E_b \qquad (2)$$

where $M''$and M' are the first and second order time
constants of the amplifier and G is the gain. E_b is the
offset voltage of the amplifier which can be adjusted
to ensure a stable operation.

The wire equation has been modified to consider a nondimensional calibration law for the convective heat transfer ($Nu = f(Re)$ instead of $E = f(U)$). The equation can be expressed as follows:

$$\frac{m_w c_w}{aR_{ref}}\frac{dR_w}{dt} = E^2\frac{R_w}{(R_1 + r_L + R_w)^2} - \pi l_w k Nu a_w R_{ref}(R_w - R_0) \qquad (3)$$

The LHS expresses the heat accumulation in the wire, while at the RHS the first term expresses the Joule heating and the second term the convection losses. R_w is the instantaneous wire resistance, R_{ref} is the wire resistance at a reference temperature of $T_{ref} = 20\,°C$ and R_0 is the resistance of the wire when it is placed unheated in the flow. It is defined as: $R_0 = R_{ref}(1 + a_w(T_0 - T_{ref}))$ where T_0 is the total temperature of the flow and a_w is the wire material's temperature coefficient of resistance.

Equations (1) – (3) form a system of non-linear ODEs which is solved with a 4th order Runge-Kutta method. The forcing function is the Nusselt number Nu(t) which is related to the flow conditions using the following correlation [3]:

$$Nu(t) = 0.42\mathrm{Pr}^{0.2} + 0.57Pr^{0.33}Re(t)^{0.5} \qquad (4)$$

For a constant Prandtl number (given fluid and small temperature variations), $Nu(t) = f(Re(t))$. The Reynolds number is based on the wire diameter.

Model parameters

The model parameters are defined by the wire properties and the circuit adjustment. A tungsten wire with a diameter of $d_w = 5\ \mu m$ and length of $l_w = 1\ mm$ is considered. The corresponding mass, temperature coefficient of resistance, heat capacity and reference resistance are as follows: $m_w = 3.78 \cdot 10^{-10}\ kg/m^3$, $a_w = 0.0036\ K^{-1}$, $c_w = 133.9\ J/kg \cdot K$, $R_{ref} = 3\ Ohm$. The resistances R_1 and R_2 depend on the anemometer. In this case, a top resistance of $R_1 = 20\ Ohm$ is used and a bridge ratio of 20, which leads to $R_2 = 400\ Ohm$. The overheat ratio OHR ($OHR = \frac{R^* - R_{ref}}{R_{ref}}$) is set to 0.58 which corresponds to an operating wire resistance of $R^* = 4.748\ Ohm$ and an operating temperature of $T_w = 455\ K$. The resistance of the prongs, stem and cable is set to $r_L = 1.63\ Ohm$ and the decade resistance is set as: $R_{dec} = 20 \cdot (r_L + R^*) = 127.56\ Ohm$.

The parameters G, M'', M', M_b and E_b determine the dynamic behavior of the system for fixed wire properties. According to Freymuth [11] and Weiss et al. [12], the cut-off frequency of the anemometer is determined by the time constant $(MM''/G)^{1/3}$. M is the wire time constant defined as:

$$M = \frac{1}{2}\frac{(R_1 + R^* + r_L)^2}{R_1}\frac{m_w c_w}{f(Re)\pi l_w k(R^* - R_0)} \qquad (5)$$

and M'' and G are characteristics of the anemometer's amplifier. In our case, since M is fixed, $M''$and G are varied to change the cut-off frequency of the system. Assuming that the amplifier consists of two identical stages, the first order time constant is computed as $M' = 0.5\sqrt{M''}$. M_b and E_b can be adjusted to optimize the dynamic response. For a maximally flat frequency response, M_b and E_b are computed as can be seen in Freymuth [11] and Weiss et al. [12].

In the present case, the anemometer is optimized for flow conditions of $Mach = 0.2$ and $T0 = 300\,K$ which correspond to a Reynolds number of $Re = 22$. Three different anemometer circuits are considered to evaluate the effect of the system's cut-off frequency to the results. Their parameters are given in Table 1.

Table 1: Parameters of CTA systems

	CTA no		
	1	**2**	**3**
f_{cut} $[kHz]$	34	44	57
G	755	1100	1820
M'' $[s]$	$5.2\ 10^{-12}$	$2.9\ 10^{-12}$	$1.9\ 10^{-12}$
M' $[s]$	$4.5\ 10^{-6}$	$3.5\ 10^{-6}$	$2.8\ 10^{-6}$
M_b $[s]$	$5.9\ 10^{-10}$	$2.1\ 10^{-10}$	$-5.3\ 10^{-11}$
E_b [V]	3.7	3.97	4.87

The cut-off frequency is the frequency corresponding to a signal attenuation of -3 dB. The system's transfer function is evaluated by its response to a Reynolds impulse. The corresponding transfer functions are presented in Figure 2.

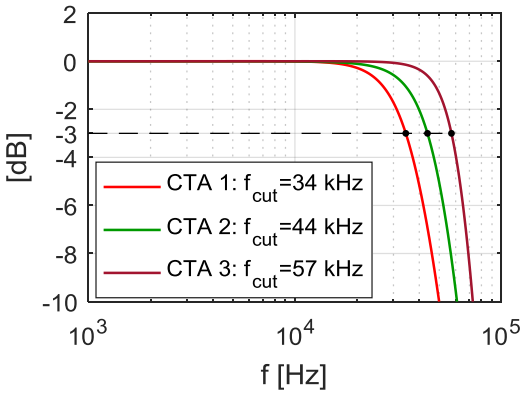

Figure 2: CTAs amplitude transfer function

SYNTHETIC TURBULENCE SIGNAL

In order to create a realistic turbulent velocity signal as input to the dynamic response model, a theoretical model for the turbulence energy spectrum is used. Pope's [15] model is employed, which expresses the 3D turbulent kinetic energy as a function of wave number:

$$E_{33}(\kappa) = C\varepsilon^{\frac{2}{3}}k^{-\frac{5}{3}}f_L(\kappa L)f_\eta(\kappa\eta) \qquad (6)$$

where f_L and f_η are functions defining the shape of the energy-containing and dissipation range respectively and are defined as:

$$f_L(\kappa L) = \left(\frac{\kappa L}{[(\kappa L)^2 + c_L]^{1/2}}\right)^{\frac{5}{3}+p_0} \qquad (7)$$

$$f_\eta(\kappa\eta) = \exp(-\beta([(\kappa\eta)^4 + {c_\eta}^4]^{\frac{1}{4}} - c_\eta)) \qquad (8)$$

The inputs that define the shape of the 1d turbulence spectrum are the turbulence intensity Tu (based on the longitudinal velocity), the integral length scale L and the kinematic viscosity ν, which is defined by the mean flow properties. These properties can be linked to the turbulent kinetic energy k, the dissipation ε and the Kolmogorov length scale η, assuming isotropic turbulence and using scaling laws:

$$Tu = \frac{\sqrt{2k/3}}{\bar{U}} \qquad (9)$$

$$L = \frac{k^{2/3}}{\varepsilon} \qquad (10)$$

$$\frac{\eta}{L} = {Re_L}^{-3/4} \qquad (11)$$

where Re_L is the Reynolds number based on the integral length scale. The 3D turbulence spectrum can now be computed by eq. (6), where $C = 1.5$, $\beta = 5.2$ and $p_0 = 2$ are empirically defined constants and $c_\eta \approx 0.4$, $c_L = 6.78$ for high Reynolds number.

For isotropic turbulence, the 1d turbulence spectrum can be computed as:

$$E_{11}(\kappa_1) = \int_{\kappa_1}^{\infty} \frac{E_{33}(\kappa)}{\kappa}\left(1 - \frac{\kappa_1^2}{\kappa^2}\right)d\kappa \qquad (12)$$

Using Taylor's [16] frozen vortex hypothesis, $(f = \frac{\kappa_1 \cdot U}{2\pi})$ the spectrum can be expressed in terms of frequency. The velocity time signal can then be retrieved by the inverse FFT of the complex signal $z = r(cos(\varphi) + i \cdot sin(\varphi))$ The amplitude r is retrieved by the energy spectrum and random phase values are generated, uniformly distributed between 0 and 2π.

Examples of the resulting 1d turbulence spectrum and velocity signal for different values of turbulence intensity and length scales are presented in Figure 3 and Figure 4. It can be seen that for the same turbulence intensity and smaller length scale, the high energy region of the spectrum has a lower energy content but extends to higher frequencies. In other words, for small integral length scales the large-amplitude fluctuations are faster.

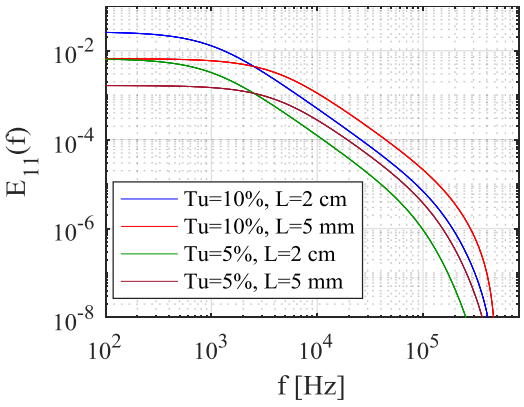

Figure 3: 1d spectrum for different values of turbulence intensity and integral length scale

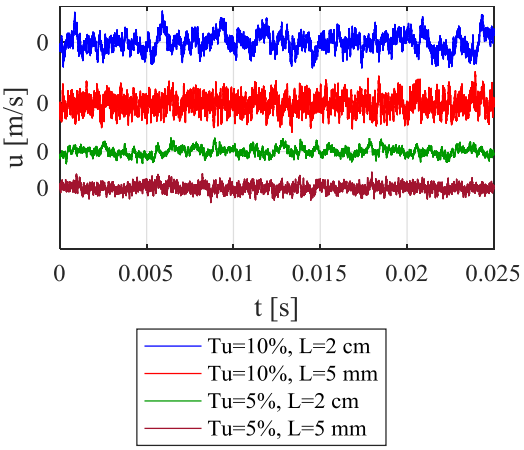

Figure 4: Turbulent velocity time series for different values of turbulence intensity and length scales

RESULTS AND DISCUSSION

Synthetic turbulence fluctuations generated with the method previously explained are superimposed to a uniform mean flow of $Mach = 0.2$ and $T0 = 300\,K$. The turbulence intensity varies between 0.5% and 22%, while the integral length scale between 0.78 mm and 2.3 cm. The synthetic velocity signal is used to create a synthetic Reynolds number $Re(t)$, and using Eq. (4), the forcing function $Nu(t)$. The system of equations (1) - (3) is then solved for all 3 anemometers and the output signal is compared to the input. The errors on the measured fluctuations' rms, integral length scale and skewness due to the CTHWA dynamic response are evaluated.

Errors as a function of input Tu and L

In this section, the errors on the measured turbulence quantities are evaluated as a function of the input turbulence level and length scale for a given anemometer. CTA 1 is selected as it features the lowest cut-off frequency ($34\,kHz$) and thus represents the most critical case.

The root mean square of the velocity fluctuations, $\overline{u'}$, is defined as:

$$\overline{u'} = \left[\frac{1}{\Delta T}\int_{t_0}^{t_0+\Delta T}(U(t)-\overline{U})^2\,dt\right]^{1/2} \qquad (13)$$

The relative error on $\overline{u'}_{out}$ is presented in Figure 5 for CTA 1, where the relative error for a parameter x is defined as:

$$error_{x,out} = 100\%\,\frac{abs(x_{in}-x_{out})}{x_{in}} \qquad (14)$$

It can be seen that the error increases for smaller length scales. As previously observed, this is explained by the extension of the high energy region of the spectrum to higher frequencies. The error is also a function of the turbulence intensity for small values but reaches a plateau for $Tu_{in} >$ 2.5%. To better understand this behavior, the input and output energy spectrum for L=1.8 mm and the first three turbulence levels are presented in Figure 6. The amplitude transfer function for CTA 1 is given as well. The input and output spectra match well, until the frequency for which attenuation starts, as indicated by the transfer function. The underestimation of $\overline{u'}$ is therefore due to the limited bandwidth of the CTA system which leads to attenuation of the output signal at high frequencies.

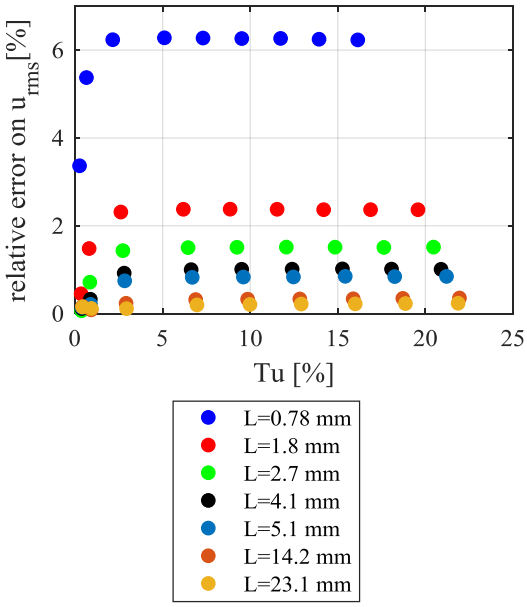

Figure 5: Relative error on the rms of the fluctuations for CTA 1 ($f_{cut} = 34\,kHz$) as a function of input Tu and L.

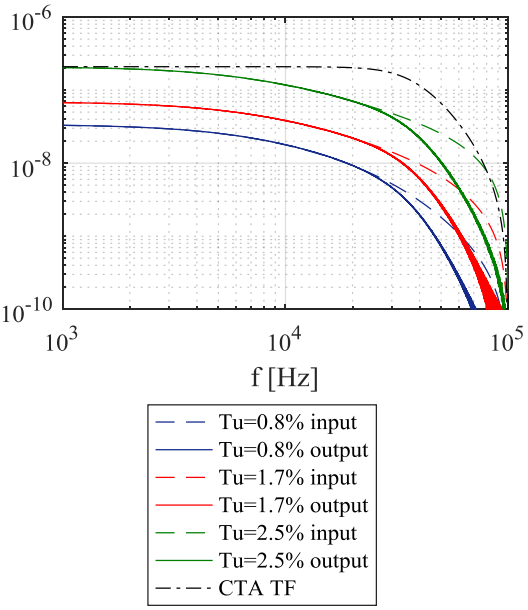

Figure 6: Input and output turbulence energy spectrum for L=1.8 mm and three turbulence levels.

In temporal measurements, the integral length scale can be computed using Taylor's frozen vortex hypothesis [16], by multiplying the integral time

scale by a convective velocity, which is usually considered equal to the local mean velocity. The integral time scale T expresses the time interval for which the velocity signal is correlated and can be computed as:

$$T = \int_0^\infty \rho(\tau) d\tau \qquad (15)$$

where $\rho(\tau)$ is the autocorrelation coefficient:

$$\rho(\tau) = \frac{\overline{u(t)u(t+\tau)}}{\overline{u^2(t)}} \qquad (16)$$

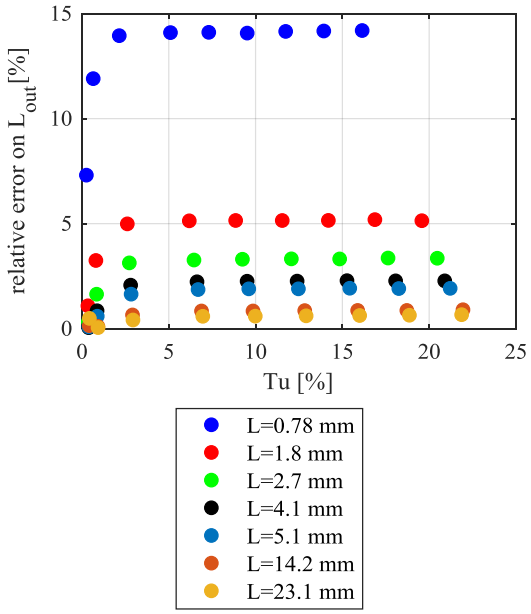

Figure 7: Relative error on the output length scale for CTA 1 , as a function of input Tu and L

The relative error on the output length scale as a function of turbulence level and input length scale is presented in Figure 7 for CTA 1. It features a similar behavior to the error in $\overline{u'}$. This is due to small differences between the input and output autocorrelation functions at short time lags.

The third order central moment, or skewness, is a measure of the lack of symmetry of the distribution and is zero for a symmetric distribution. It is computed as:

$$skew = \frac{1}{\overline{u'}^3}\frac{1}{\Delta T}\int_{t_0}^{t_0+\Delta T} (U(t) - \overline{U})^3\, dt \qquad (17)$$

The absolute error for the output skewness is presented in Figure 8. The absolute error is presented instead of the relative one, as the relative does not show a clear trend with respect to the input parameters. Moreover, this allows to compare with the results of Weiss et al. [12]. It is verified that the skewness is increased by the presence of large fluctuations at high frequencies, as a clear dependency on Tu and L can be seen.

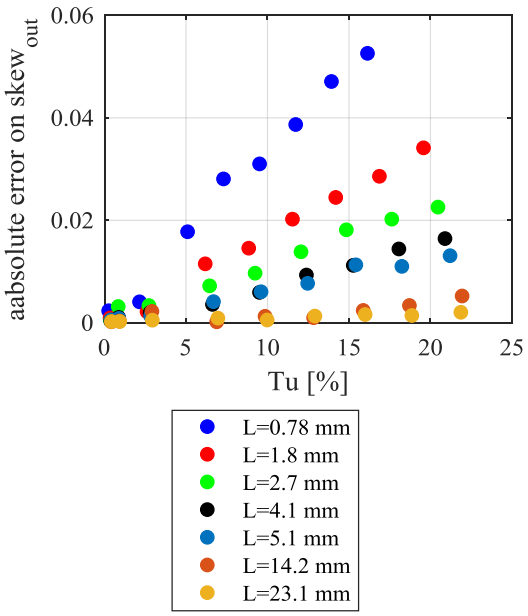

Figure 8: Absolute error on the output skewness for CTA 2 , as a function of input Tu and L

Errors as a function of the anemometer's cut-off

In this section, the results of all the anemometers are considered. As expected, the anemometers with higher cut-off frequency perform better and feature reduced errors. The critical parameters are the position of the cut-off relative to the shape of the turbulence spectrum and the turbulence level. Therefore, the errors are plotted as a function of Tu and f_L/f_{cut}, where $f_L = \overline{U}/L$ is a characteristic frequency of the spectrum which corresponds approximately to the middle of the inertial range.

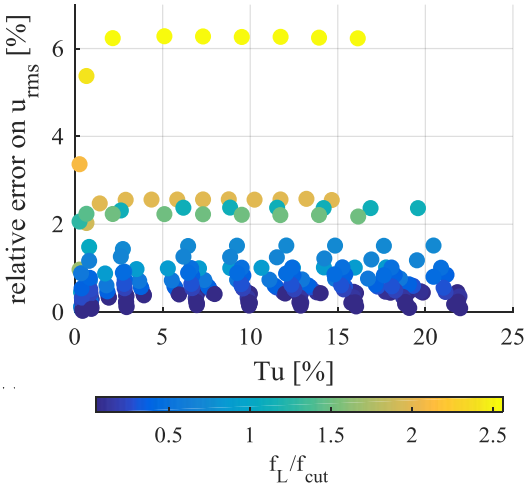

Figure 9: Relative error on the rms of the fluctuations for all anemometers as a function of input Tu and f_L/f_{cut}.

The relative errors on $\overline{u'}$ and L and the absolute error on the skewness are presented in Figures 9 – 11. The same trend is observed overall

as in the previous section for CTA 1. Therefore, we can use these results to evaluate the magnitude of errors for turbulence measurements with optimally adjusted anemometers (for maximally flat frequency response). Two turbomachinery related examples are presented in the next subsection.

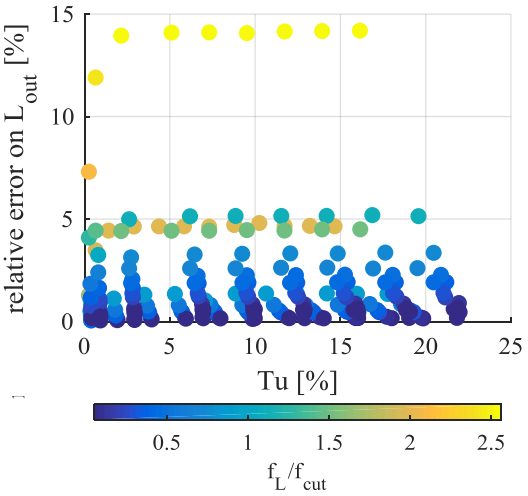

Figure 10: Relative error on the integral length scale for all anemometers as a function of input Tu and f_L/f_{cut}.

Application examples

The results of the previous analysis can be used to define the instrument's bandwidth requirements for a specific application or they can be employed in the framework of an uncertainty analysis after measurements have been performed. This will be demonstrated for two typical examples of laboratory flows.

The first case is high-intensity, large-scale inlet turbulence for wind tunnel testing of high pressure turbine blades. For representative heat transfer measurements, the turbulence field at the combustor exit must be simulated, which is characterized by high turbulence intensity and large length scales. Many works exist in the literature, for example Ames & Plesniak [17] and van Fossen et al. [18]. The turbulent field characteristics for these works are $Tu = 28.5\% - L = 3.3\ cm$ and $Tu = 12\ \% - L = 3.3\ cm$ respectively. Assuming three different inlet Mach numbers of 0.1, 0.15 and 0.2 and ambient temperature, the characteristic frequency f_L can be computed for each condition as 1 kHz, 1.5 kHz and 2 kHz respectively. In this case, even for a CTHWA with a low cut-off frequency of 15 kHz, the parameter f_L/f_{cut} ranges from 0.067 – 0.13. As can be seen from Figures 9 and 10, the error is negligible for both $\overline{u'}$ and L, for both turbulence levels considered. From Figure 11 we can see that the error in the skewness is less than 0.002 for Tu=12% and less than 0.01 by extrapolating to Tu=28%. Despite the high turbulence levels, this case is rather favorable. Thanks to the large length scales and the low mean velocities, the high energy content is restricted to the low frequency range and the errors due to the dynamic response are minimized.

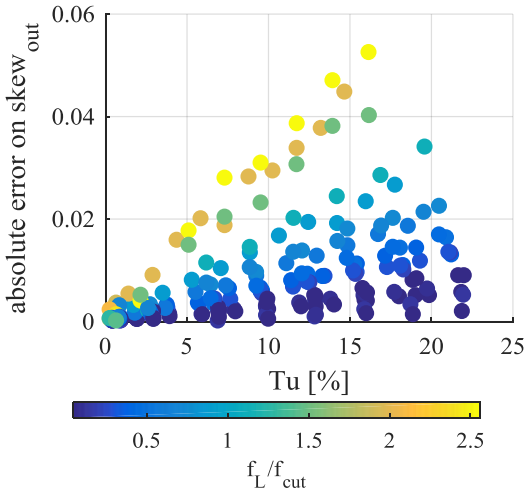

Figure 11: Absolute error on the output skewness for all anemometers, as a function of input Tu and f_L/f_{cut}.

The second case is turbulence measurements inside a blade wake. This case is characterized by high turbulence intensity (in the range of 10-15%, e.g. in [19]) but small length scales, of the order of magnitude of the trailing edge thickness. The Mach number can vary significantly depending on low-speed or high-speed testing. For a turbulence intensity level of 10%, a length scale of 2 mm and a Mach number of 0.3, the characteristic frequency f_L is equal to 51.5 kHz. From Figures 9 and 10 it can be seen that to keep the error on $\overline{u'}$ less than 1%, f_L/f_{cut} must be lower than 1 and f_{cut} must be at least 51.5 kHz. For the same f_{cut}, the error on L is around 3-4%. Finally, the absolute error on the skewness is around 0.01 from Figure 11. This case is more problematic due to the small length scales, as a significant part of the spectrum extends in the high frequency range. Anemometers with high frequency response should be used and the magnitude of possible errors should be evaluated.

In this section, two turbomachinery flow examples have been used to illustrate how the results of the previous analysis could be exploited. Before being universally used, it must be remembered that the analysis is based on a simplified anemometer circuit and optimally adjusted anemometers for maximally flat frequency response. Nevertheless, it is believed that a good estimate of the errors can be provided in any case.

CONCLUSIONS

Synthetic turbulence signals of varying turbulence levels and length scales are used together with a non-linear dynamic response model to evaluate the effects of the dynamic response of CTHWA on the measurement of turbulence

parameters. Errors due to limited bandwidth and non-linearity are considered. The latter has been shown to be important for large-amplitude and high frequency fluctuations as the ones encountered in turbomachinery flows.

The results show that the errors in the measurement of the rms of the turbulence fluctuations and the integral length scale, mainly occur due to the limited bandwidth of the instrument and are a function of the ratio f_L/f_{cut}, where f_L is a characteristic frequency of the turbulence spectrum and f_{cut} the cut-off frequency of the anemometer. The error on the skewness is affected both by f_L/f_{cut} and the turbulence level, and stems from the non-linearity of the system. The effect of the cut-off frequency of the anemometer is examined by considering three anemometers with the same wire but different amplifier characteristics. All three are optimally adjusted for maximally flat response following Freymuth [11] and Weiss et al. [12].

Two turbomachinery flow examples are used to illustrate the importance of this analysis: high-intensity, large-scale turbulence typical of the inlet flow for high pressure turbine wind tunnel testing, and blade wake turbulence, characterized by high intensity and small length scales. The second case is more critical for errors stemming from the dynamic response, due to the small-scale turbulence where the high energy range extends to higher frequencies.

This analysis can be used to evaluate the errors stemming from the dynamic response of CTHWAs or used to select appropriate instruments in order to minimize such errors. The continuation of this work will include rotor flows with different turbulence contents, to evaluate the dynamic response errors at the more challenging conditions of rotating wake flow.

ACKNOWLEDGMENTS

The first author greatly acknowledges the support of the Fonds de la Recherche Scientifique - FNRS, through the award of a FRIA doctoral grant.

REFERENCES

[1] Mayle, R. E.; Dullenkopf, K. and Schulz, A.; 1998. “1997 Best Paper Award—Heat Transfer Committee: The Turbulence That Matters”. Journal of Turbomachinery, 120(3), p.402

[2] Sagaut, P. and Deck, S.; 2009. “Large eddy simulation for aerodynamics: status and perspectives”. Philosophical Transactions of the Royal Society A: Mathematical, Physical and Engineering Sciences, 367(1899), pp.2849-2860

[3] Bruun, H. H.; 1995. “Hot-wire anemometry”. Oxford: Oxford University Press

[4] Comte-Bellot, G.; 2007. “Thermal Anemometry”. In: Tropea, C. A.; Yarin, A. L. and Foss, J. F. (eds) Springer Handbook of Experimental Fluid Mechanics. Springer-Verlag, pp. 229-287

[5] Ligrani, P. M. and Bradshaw, P.; 1987. “Spatial resolution and measurement of turbulence in the viscous sublayer using subminiature hot-wire probes”. Experiments in Fluids, 5, pp. 407-417

[6] Hultmark, M.; Ashok, A. and Smits, A.; 2011. “A new criterion for end-conduction effects in hot-wire anemometry”. Measurement Science and Technology, 22(5), p.055401

[7] Li, J. D.; 2007. “Hot-wire attenuation and its correction in turbulence measurements”. 16th Australasian Fluid Mechanics Conference, Univ. of Queensland, Australia

[8] Weiss, J.; Knauss, H. and Wagner, S.; 2001. “Method for the determination of frequency response and signal to noise ratio for constant-temperature hot-wire anemometers”. Review of Scientific Instruments, 72(3), p.1904

[9] Freymuth, P.; 1977. “Frequency response and electronic testing for constant-temperature hot-wire anemometers”. Journal of Physics E: Scientific Instruments, 10(7), pp.705-710

[10] Berson, A.; Blanc-Benon, P. and Comte-Bellot, G. 2010. “On the use of hot-wire anemometry in pulsating flows”. A comment on ‘A critical review on advanced velocity measurement techniques in pulsating flows’. Measurement Science and Technology, 21(12), p.128001

[11] Freymuth, P.; 1977. “Further investigation of the nonlinear theory for constant-temperature hot-wire anemometers”. Journal of Physics E: Scientific Instruments, 10(7), pp.710-713

[12] Weiss, J.; Berson, A. and Comte-Bellot, G.; 2013. “Investigation of nonlinear effects in constant-temperature anemometers”. Measurement Science and Technology, 24(8), p.085302

[13] Comte-Bellot, G. and Schon, J.; 1969. “Harmoniques créés par excitation paramétrique dans les anémomètres à fil chaud a intensité constante ». International Journal of Heat and Mass Transfer, 12(12), pp.1661-1677

[14] Berson, A.; Blanc-Benon, P. and Comte-Bellot, G.;2009. “A strategy to eliminate all nonlinear effects in constant-voltage hot-wire anemometry”. Review of Scientific Instruments, 80(4), p.045102

[15] Pope, S.; 2000. “The scales of turbulent motion. Turbulent Flows”. pp.182-263

[16] Taylor, G. I.; 1938. "The spectrum of turbulence". Proc. R. Soc. Lond. 164 (919), pp. 476–490

[17] Ames, F. and Plesniak, M.; 1997. "The influence of large-Scale, high-intensity turbulence on vane aerodynamic losses, wake growth, and the exit turbulence parameters". Journal of Turbomachinery, 119(2), p.182

[18] Van Fossen, G. and Bunker, R.; 2001. "Augmentation of stagnation region heat transfer due to turbulence from a DLN can combustor". Journal of Turbomachinery, 123(1), p.140

[19] Boyle, R.; Lucci, B. and Senyitko, R. 2002. "Aerodynamic performance and turbulence measurements in a turbine vane cascade". In: ASME Turbo Expo 2002: Power for Land, Sea, and Air